JOURNAL OF AIRCRAFT
Vol. 51, No. 6, November–December 2014

Theoretical and Experimental Results for the S414, Slotted, Natural-Laminar-Flow Airfoil

James G. Coder* and Mark D. Maughmer†
Pennsylvania State University, University Park, Pennsylvania 16802
and
Dan M. Somers‡
Airfoils, Incorporated, Port Matilda, Pennsylvania 16870

DOI: 10.2514/1.C032566

The S414, slotted, natural-laminar-flow airfoil was designed for rotorcraft applications and has been analyzed theoretically using MSES and OVERFLOW. In addition, it has been verified experimentally in the Pennsylvania State University Low-Speed, Low-Turbulence Wind Tunnel. The primary objectives of the design are high maximum lift and low profile drag, both of which have been achieved while satisfying a thickness constraint. The theoretical analyses show good agreement with the experimental results. The experimental results are compared with those of the S406 and S411 airfoils, which were designed to similar specifications, and illustrate the potential benefits of the slotted, natural-laminar-flow concept.

Nomenclature

C_p	=	$(p_l - p_\infty)/q_\infty$, pressure coefficient
c	=	airfoil chord
c_d	=	section profile-drag coefficient
c_l	=	section lift coefficient
c_m	=	section pitching-moment coefficient about the quarter-chord point
p	=	static pressure
q	=	dynamic pressure
R	=	Reynolds number based on airfoil chord and freestream conditions
x	=	airfoil abscissa
α	=	angle of attack

Subscripts

l	=	local point on airfoil
∞	=	freestream conditions

I. Introduction

THE slotted, natural-laminar-flow (SNLF) airfoil concept [1,2] is a design that can achieve lower profile-drag coefficients by allowing natural laminar flow to be extended beyond the limits typically present on single-element airfoils. The two-element, SNLF airfoil concept is similar in nature to the slotted, supercritical airfoil concept [3] in that it employs a slot to achieve a pressure recovery that would not be possible on a single-element airfoil.

The aft element eliminates the requirement that the pressure at the trailing edge of the fore element recover to the freestream; thus, the favorable pressure gradient can extend farther aft on the fore element than would otherwise be the case. When operating in the low-drag range, the SNLF airfoil concept has favorable gradients extending along both surfaces of the fore element to near its trailing edge. Thus, the fore element is entirely laminar. The aft element then provides the necessary recovery to freestream pressure. Because the wake of the fore element does not impinge on the aft element and because of its low Reynolds number, the aft element can also achieve significant extents of laminar flow. A conceptual surface pressure distribution near the middle of the low-drag, lift-coefficient range is illustrated in Fig. 1.

The concept exhibits low section profile-drag coefficients without having to resort to the complexity and cost of laminar flow control, and it also achieves a high maximum lift coefficient without variable geometry (i.e., the aft element need not be deflected). The SNLF airfoil shape is not radically different from conventional airfoil shapes, no more than conventional, natural-laminar-flow airfoil shapes are from conventional, turbulent-flow airfoil shapes. Unlike conventional airfoils with slotted flaps, however, the SNLF airfoil is not a nested configuration; the slot between the fore and aft elements is always open.

Although the SNLF concept is suited to a wide range of applications and operating conditions, the airfoil that is the focus of the current investigation, designated the S414 [4], was specially designed for the rotor of a small helicopter having a torsionally stiff blade capable of handling much larger pitching moments than historically accepted. An investigation was conducted in the Pennsylvania State University Low-Speed, Low-Turbulence Wind Tunnel to obtain the basic, low-speed, two-dimensional characteristics of the airfoil. These results have been compared with predictions from two different theoretical methods. The experimental results have also been compared with those obtained in the same wind tunnel for the S406 [5] and S411 [6] airfoils, both of which have design specifications similar to those of the S414 airfoil.

II. Design

The S414 airfoil was designed to satisfy two primary objectives [4]. The first was that the airfoil should achieve a maximum lift coefficient of 1.25 at a Mach number of 0.30 and a Reynolds number of 0.97×10^6, and a maximum lift coefficient of 1.20 at a Mach number of 0.40 and a Reynolds number of 1.29×10^6. These maximum lift coefficients should not show a significant decrease if transition is fixed near the leading edge of either or both elements. The second objective was that low profile-drag coefficients be exhibited from a lift coefficient of 0.10 at a Mach number of 0.70 and a Reynolds number of 2.26×10^6 to a lift coefficient of 0.65 at a Mach number of 0.45 and a Reynolds number of 1.45×10^6. A constraint

Presented as Paper 2013-2407 at the 31st AIAA Applied Aerodynamics Conference, San Diego, CA, 24–27 June 2013; received 7 August 2013; revision received 29 July 2014; accepted for publication 2 August 2014; published online 29 October 2014.

*Graduate Assistant, Department of Aerospace Engineering, 229 Hammond Building. Student Member AIAA.
†Professor, Department of Aerospace Engineering, 229 Hammond Building. Associate Fellow AIAA.
‡President, 122 Rose Drive.

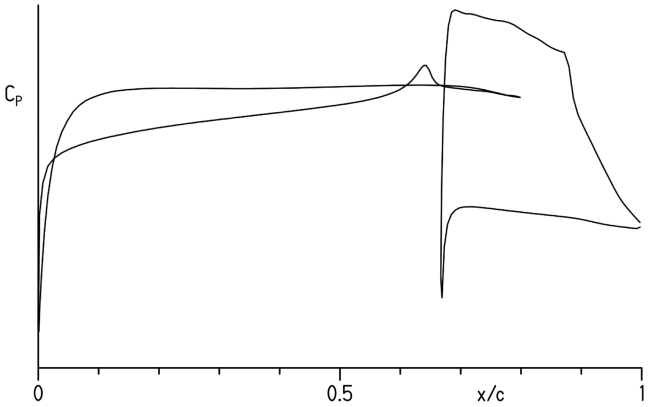

Fig. 1 Sketch of the pressure distribution near the middle of the low-drag, lift-coefficient range.

on the design was that the thickness should be approximately 14% chord.

The design specifications for the S414 airfoil are similar to those for the single-element S406 airfoil [5] and identical to those for the single-element S411 airfoil [6]; however, the S414 airfoil had no constraint on the zero-lift pitching-moment coefficient.

The initial fore- and aft-element shapes were designed using the Eppler Airfoil Design and Analysis Code [7,8]. The Eppler code is a subsonic single-element code that consists of an inverse conformal mapping method for design and a panel method coupled with an integral boundary-layer method for analysis. The fore-element shape was refined using the MSES code [9], which is capable of analyzing multi-element airfoils. For the purpose of testing this airfoil at Mach numbers below the design conditions, the aft half of the lower surface of the fore element was modified, resulting in the airfoil being thinner around the entry to the slot. The modification allows the geometry to exhibit the pressure gradients that would be present at the higher design Mach numbers. Otherwise, the pressure gradients around the entrance to the slot would be unfavorable with respect to laminar flow at the test Mach numbers. The airfoil shape as tested is shown in Fig. 2. This test shape was used for all theoretical analyses included in this paper.

III. Theoretical Analysis Methods

A. MSES 3.05

The MSES code [9] combines an Euler solver for the outer flow and an integral boundary-layer method for the viscous layer and is capable of analyzing multi-element airfoils. As an upwind Euler method, it is able to predict the aerodynamic characteristics of airfoils in the transonic regime.

The boundary-layer solver can predict transition using a full e^N method, in which a Newton iteration method is used to find the critical Tollmien–Schlichting frequency [10], or by means of the approximate envelope e^N method [11]. The predictions presented here use the full e^N method, whereas those obtained using the approximate envelope method can be found in [4]. For the present calculations, the critical amplification factor was set to 9.

B. OVERFLOW 2.2e

OVERFLOW [12] is a structured-overset, three-dimensional Reynolds-averaged Navier–Stokes (RANS) solver that is also capable of two-dimensional analysis. A wide variety of solution methods and turbulence models are available in the solver. For the present study, a third-order-accurate upwind Roe scheme [13] is used with scalar-pentadiagonal solution advancement [14] and low-Mach preconditioning [15]. The solutions are run non-time-accurate until force/moment convergence is achieved (typically coinciding with the residuals approaching machine-level zero). RANS closure was achieved using the Spalart–Allmaras turbulence model [16] and the transition model developed by Coder and Maughmer [17], which is based on the approximate envelope transition method [11]. The freestream modified-eddy-viscosity ratio was set to 0.1 (an actual eddy-viscosity ratio of 2.8×10^{-7}), which provides an essentially laminar freestream. The turbulence intensity was set to 0.045%, which is representative of the test facility flow quality.

The overset computational mesh for the S414 airfoil was generated using Chimera Grid Tools [18]. The surface definitions were refined such that each element has approximately 400 points along its surface. The volume grids for each element were generated separately following the best practices in overset grid generation [19] with a background box grid.

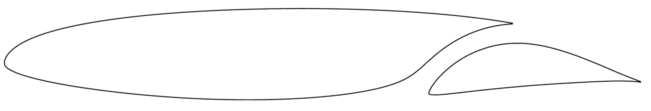

Fig. 2 S414 slotted, natural-laminar-flow airfoil.

IV. Experimental Procedure

A. Facility Description

The S414 airfoil has been tested in the Penn State University Low-Speed, Low-Turbulence Wind Tunnel (LSLTT), which is a closed-throat, single-return atmospheric facility. The test section is rectangular and is 101.3 cm (39.9 in.) high and 147.6 cm (58.1 in.) wide with filleted corners. The maximum test-section speed is 67 m/s (220 ft/s). Airfoil models are mounted vertically in the test section and attached to computer-controlled turntables that allow the angle of attack to be set. The turntables are flush with the floor and ceiling and rotate with the model. The flow quality of the Penn State LSLTT has been measured and documented [20]. At a velocity of 46 m/s (150 ft/s), the flow angularity in the test section is everywhere below ± 0.25 deg, the mean velocity variation is below $\pm 0.2\%$, and the turbulence intensity is less than 0.045%.

To obtain drag measurements, a wake-traversing Pitot-static pressure probe is mounted from the ceiling of the tunnel. A traversing mechanism incrementally positions the probe across the wake, which automatically aligns with the local wake-centerline streamline as the angle of attack changes.

The basic wind-tunnel pressures are measured using pressure-sensing diaphragm transducers. Measurements of the pressures on the model are made by an automatic pressure-scanning system. Data are obtained and recorded with an electronic data-acquisition system.

B. Model

The aluminum wind-tunnel model, pictured in Fig. 3, was fabricated by Advanced Technologies, Inc. (Newport News, Virginia), using a numerically controlled milling machine. The model has a

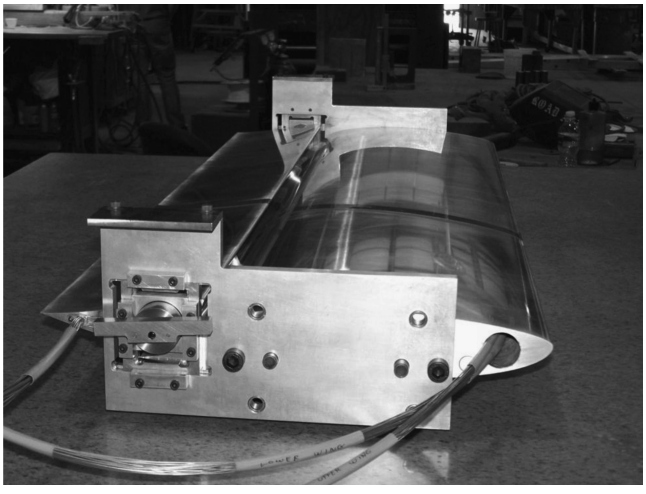

Fig. 3 Aluminum wind-tunnel model of the S414 airfoil.

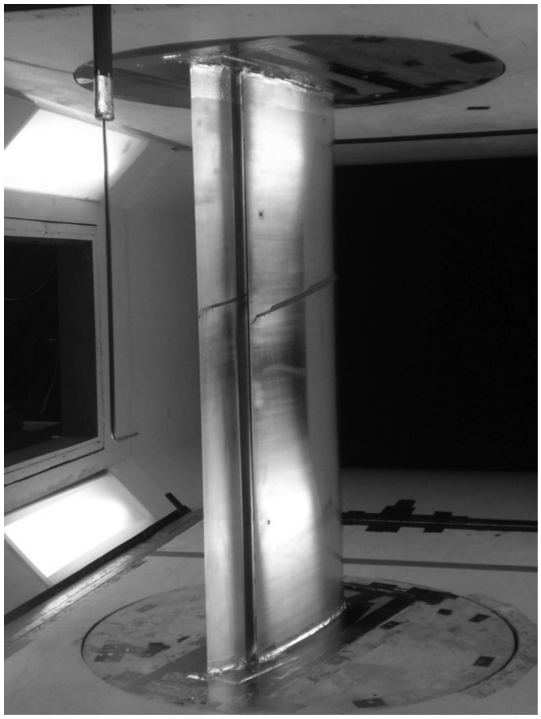

Fig. 4 S414 wind-tunnel model installed in the Pennsylvania State University Low-Speed, Low-Turbulence Wind Tunnel.

chord of 457.2 mm (18.00 in.) and a span of 107.95 cm (42.50 in.) and thus is extended through both turntables. Upper- and lower-surface pressure orifices are located to one side of midspan at staggered positions. All the orifices are 0.51 mm (0.020 in.) in diameter with their axes perpendicular to the surface. The surfaces of the model were sanded to ensure an aerodynamically smooth finish that will not cause premature transition. The measured model contour is within 0.13 mm (0.005 in.) of the prescribed shape. The model as installed in the Penn State LSLTT can be seen in Fig. 4.

C. Experimental Methods

The surface pressures measured on the model were reduced to standard pressure coefficients and numerically integrated to obtain section normal- and chord-force coefficients, as well as section pitching-moment coefficients about the quarter-chord point. Section profile-drag coefficients are computed from the wake total and static pressures using standard procedures [21]. At most poststall angles of attack, however, wake surveys are not performed, and profile-drag coefficients are computed from normal- and chord-force coefficients obtained from pressure integration. Low-speed wind-tunnel boundary corrections were applied to the data [22]. A total-pressure-tube displacement correction, although quite small, was also applied to the wake measurements [21].

The uncertainty of a measured force or moment coefficient depends on the operating conditions and generally increases with increasing angle of attack [23]. At higher lift, for which the uncertainty is greatest, the measured lift coefficients have an uncertainty of $\Delta c_l = \pm 0.005$, and the pitching-moment coefficients have an uncertainty of $\Delta c_m = \pm 0.002$. The uncertainty of the drag coefficients measured in the low-drag range is $\Delta c_d = \pm 0.00005$ (0.5 drag counts), increasing to $\Delta c_d = \pm 0.00015$ (1.5 drag counts) as the angle of attack approaches stall.

In addition to making the quantitative measurements indicated, flow-visualization studies were performed using fluorescent oil [24]. These studies were used not only to determine transition locations and regions of separated flow but also to verify the two-dimensionality of the tests. As is typical for this facility, the flow over the model was two-dimensional up to and slightly beyond the angle of attack at which the maximum lift coefficient occurs.

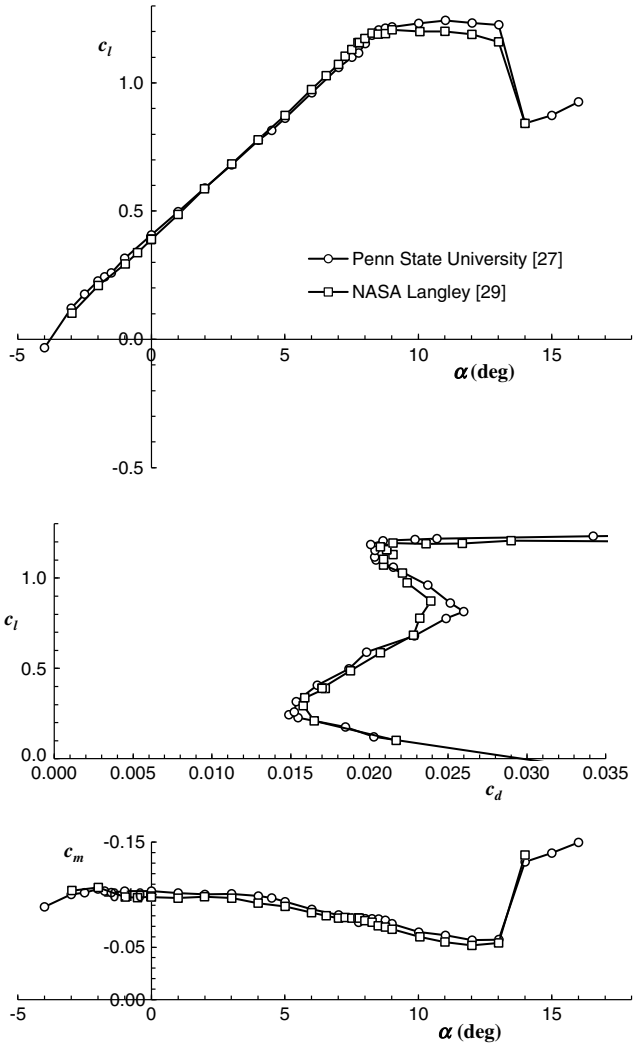

Fig. 5 Section characteristics of the E 387 airfoil measured at Penn State compared with those measured at NASA Langley for $R = 0.1 \times 10^6$.

D. Facility Qualification

Confidence in the Penn State LSLTT has been gained by making comparisons with data taken elsewhere. For this purpose, the now-defunct NASA Langley Research Center Low-Turbulence Pressure Tunnel (LTPT) [25] and the Delft University of Technology Low-Speed Wind Tunnel in The Netherlands [26] are perhaps the two most highly regarded two-dimensional, low-speed wind tunnels. Although detailed comparisons of the Penn State LSLTT with these tunnels can be found in [27,28], two such validation cases are included in this paper. For low-Reynolds-number airfoil aerodynamics, a benchmark data set is that obtained for the E 387 airfoil in LTPT [29]. In Fig. 5, these results are compared with those from the Penn State tunnel for a Reynolds number of $R = 0.1 \times 10^6$. The agreement of the data from the Penn State facility with those from LTPT is excellent.

In Fig. 6, Penn State tunnel measurements made using the laminar-flow S805 wind-turbine airfoil [28] are compared with those obtained using the same wind-tunnel model at TU Delft [30] for a Reynolds number of $R = 1.5 \times 10^6$. These data also demonstrate excellent agreement. Although not presented here, pressure distributions and measured transition locations obtained at Penn State also show excellent agreement with those of the Delft experiments [28].

V. Experimental and Theoretical Results

A. Section Characteristics

Experimentally measured section characteristics for the S414 airfoil for several Reynolds numbers ranging from $R = 0.5 \times 10^6$ to

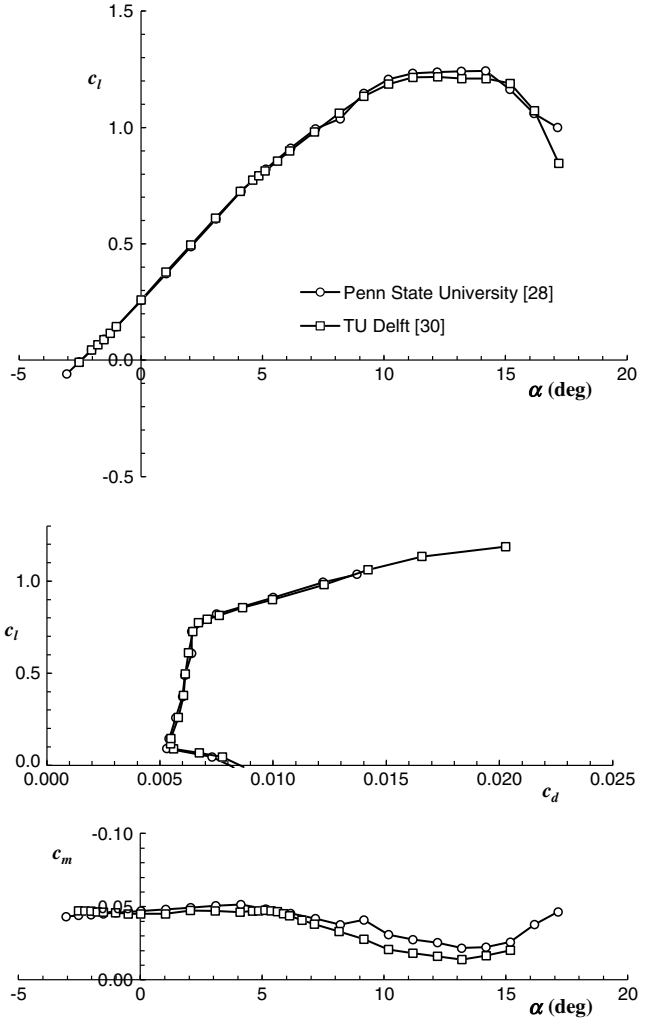

Fig. 6 Section characteristics of the S805 airfoil measured at Penn State compared with those measured at TU Delft for $R = 1.5 \times 10^6$.

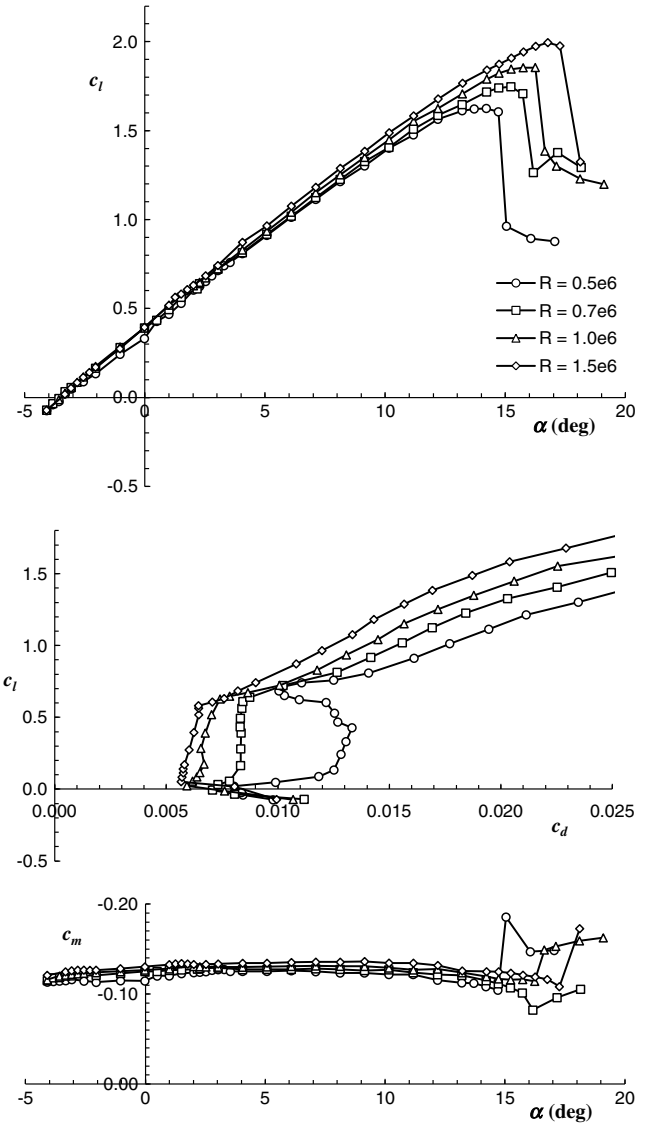

Fig. 7 Effect of Reynolds number on the free-transition experimental section characteristics.

$R = 1.5 \times 10^6$ are shown in Fig. 7. The lift-curve slope and the maximum lift coefficient both increase with Reynolds number, whereas the extent of the low-drag range decreases with increasing Reynolds number. More specifically, the lower limit increases and the upper limit decreases as Reynolds number is increased. There are unusual shapes to the drag polars at the lower Reynolds numbers. For the lowest Reynolds number $R = 0.5 \times 10^6$, the shape of the drag polar is strongly influenced by laminar-separation-bubble effects causing increased drag within the low-drag range. More notable is that there is a "horn" in the data at the lower limit of the low-drag range for $R = 0.7 \times 10^6$ where the drag coefficient drops significantly below those in the rest of the low-drag range. This feature is also present for $R = 1.0 \times 10^6$, though it is less distinct. It may also be present for the lowest Reynolds number as well, but it is tough to discern from the laminar-separation-bubble effects. The horn is probably the result of an interaction between the wake of the fore element and the laminar separation bubble on the upper surface of the aft element. At the lower limit of the low-drag range, transition on the lower surface of the fore element occurs near the trailing edge. It is likely that the resulting turbulence alleviates the separation bubble on the aft element, thereby reducing the total drag. A reduction in the length of the laminar separation bubble at the lower limit of the low-drag range has been confirmed using oil-flow visualizations [4].

Comparisons of the theoretical and experimental section characteristics of the S414 airfoil with free transition for Reynolds numbers of 0.7×10^6 and 1.5×10^6 are shown in Figs. 8, 9, respectively. The predictions from both MSES and OVERFLOW agree very well with each other for the lift, but they predict a more-negative zero-lift angle than was observed in the wind tunnel. The abruptness of the stall was captured in the OVERFLOW simulations, whereas MSES predicted a much more docile stall than was measured. Both methods overpredict the maximum lift coefficient and the slope of the lift curve. The quality of the pitching-moment-coefficient predictions is similar to that of the lift coefficients, with MSES and OVERFLOW agreeing with each other but predicting more-negative pitching moments than were measured. There is mixed agreement with experiment for the profile-drag coefficients. Both methods do well in predicting the drag levels in the low-drag range for both Reynolds numbers, though neither predicts the presence of the horn for $R = 0.7 \times 10^6$. The OVERFLOW predictions show steadily increasing profile-drag in the low-drag range for both Reynolds numbers. This is spurious drag that is a result of the solver not having far-field vortex corrections. As such, the strong agreement between OVERFLOW and experiment for $R = 1.5 \times 10^6$ may be somewhat fortuitous. The upper limit of the low-drag range is predicted by both codes to be at a higher lift coefficient than indicated by experiment. MSES predicts the lower limit of the low-drag range well, whereas OVERFLOW predicts it to occur at too low of lift coefficient.

B. Pressure Distributions

Select experimental surface pressure distributions for $R = 1.5 \times 10^6$ are plotted in Fig. 10. The angles of attack included in this

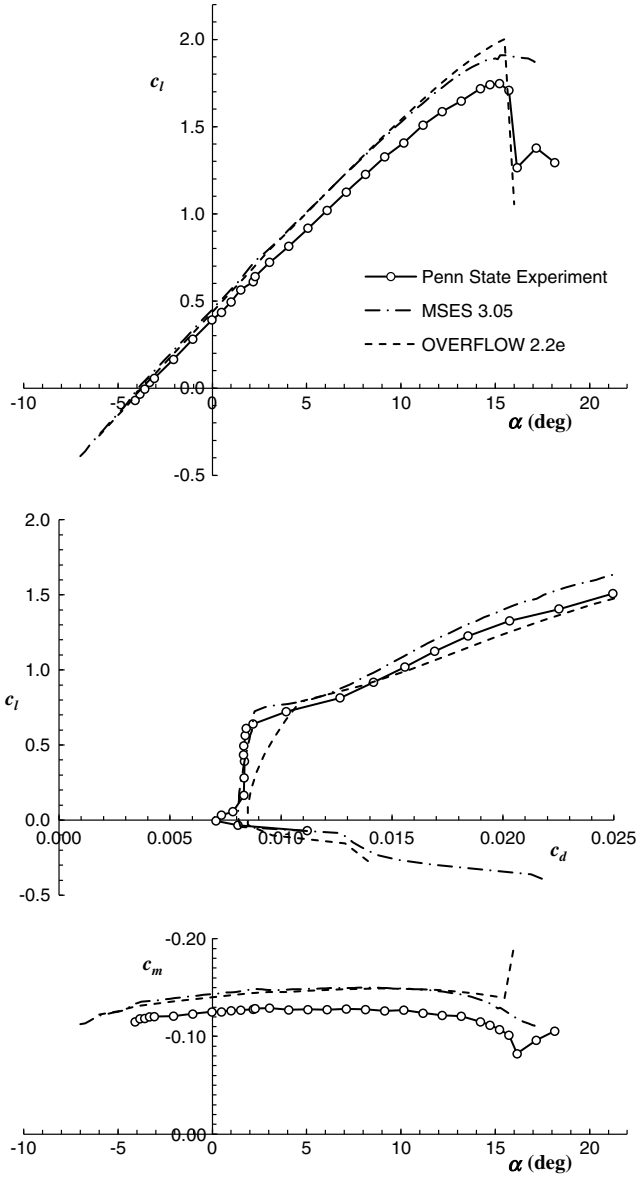

Fig. 8 Comparison of predicted and measured section characteristics for the S414 airfoil for $R = 0.7 \times 10^6$.

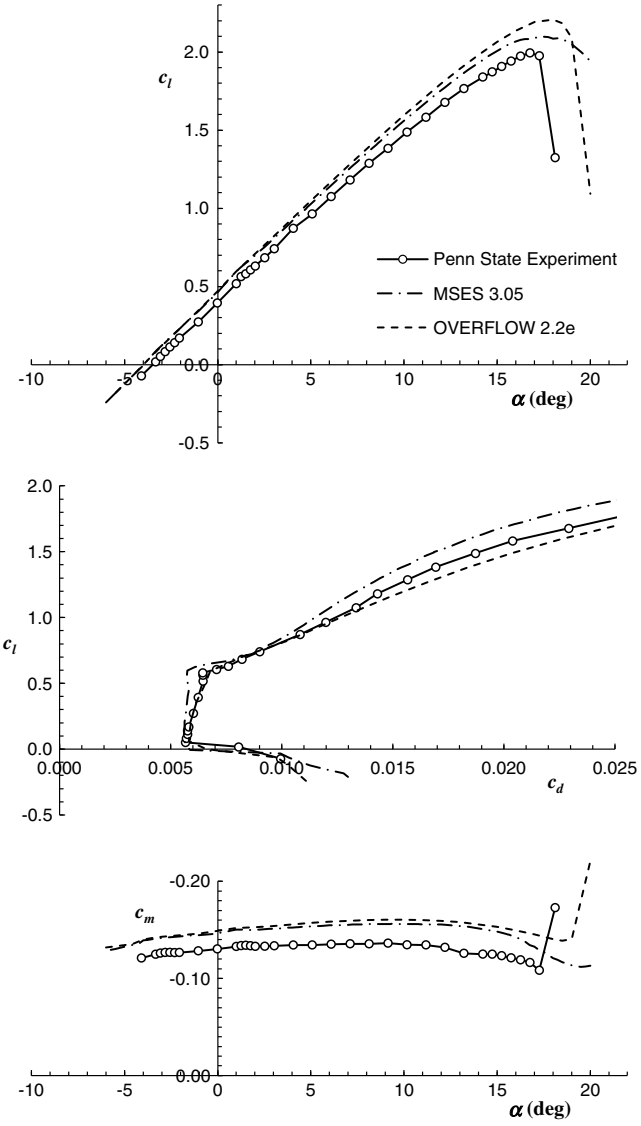

Fig. 9 Comparison of predicted and measured section characteristics for the S414 airfoil for $R = 1.5 \times 10^6$.

plot represent the lower and upper corners of the low-drag region ($c_l = 0.052$ and $c_l = 0.631$, respectively) and the maximum lift coefficient ($c_l = 1.994$) for this Reynolds number. These distributions show that almost all of the lift variation is carried on the fore element, whereas the aft element experiences a much smaller effect. The upper-surface pressure distribution on the aft element changes very little across the operational range of this airfoil.

Comparisons of measured and predicted pressure distributions are shown in Figs. 11, 12 for $R = 0.7 \times 10^6$ and $R = 1.5 \times 10^6$, respectively. In both plots, the angle of attack for the experimental data is nominally 1 deg. Because the section characteristics indicate a shift in the zero-lift angle of attack between experiment and theory, both OVERFLOW and MSES were run to match the lift coefficients for the given Reynolds numbers. For $R = 0.7 \times 10^6$ case, the lift coefficient is 0.493, whereas for $R = 1.5 \times 10^6$, the lift coefficient is 0.518. The corresponding OVERFLOW and MSES angles of attack are 0.49 and 0.36 deg, respectively, for $R = 0.7 \times 10^6$, and 0.38 and 0.41 deg, respectively, for $R = 1.5 \times 10^6$. In both cases, the OVERFLOW and MSES predictions agree exceptionally well on the fore element. The only region of discrepancy is in the entrance to the slot, but the differences are very small. Both theoretical pressure distributions predict the pressures on the fore element to be lower than actually measured in the wind tunnel. This appears to be due to differences in the pressure that is recovered at the trailing edge of the fore element, with the experiment showing a higher pressure than predicted. The theories also agree very well with each other on the aft element. They also agree well with experiment at the specified lift coefficient for $R = 0.7 \times 10^6$ but less so for $R = 1.5 \times 10^6$. The latter disagreement may be attributed to fact that these distributions match the total lift coefficient of the two elements rather than either element in particular.

Overall, the agreement of both theoretical methods is remarkably good, considering the complexity of the configuration. This comparison also validates the transitional computational-fluid-dynamics-based approaches for analyzing the SNLF concept. Computational fluid dynamics analyses will be particularly useful in the future for determining performance gains and drag penalties due to installation of this concept on an actual aircraft.

VI. Comparison with the S406 and S411 Airfoils

Because the S414 airfoil was designed for the same objectives as the S411 airfoil and similar objectives to those for the S406 airfoil, the aerodynamic benefits of the slotted, natural-laminar-flow design can be determined by comparing the section characteristics of the three airfoils. The lift, profile-drag, and pitching-moment coefficients of all

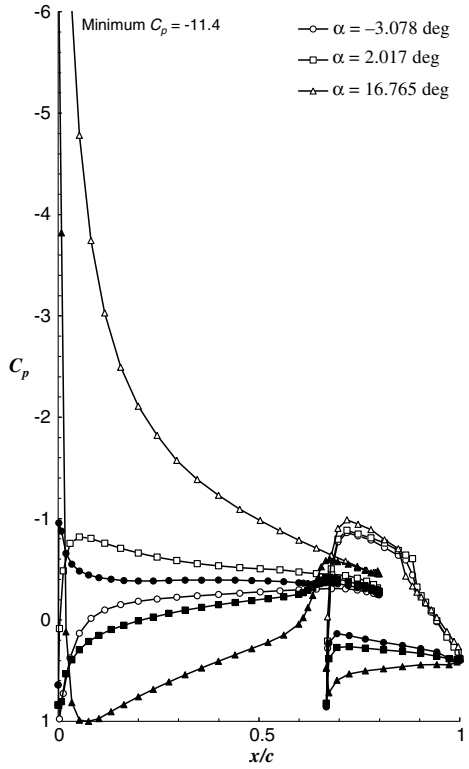

Fig. 10 Selected experimental pressure distributions for $R = 1.5 \times 10^6$ (filled symbols — lower surface; open symbols — upper surface).

three airfoils with free transition are compared for a Reynolds number of 0.7×10^6 in Fig. 13 and for $R = 1.5 \times 10^6$ in Fig. 14. The S414 airfoil exhibits profile-drag coefficients that are lower than the S411 airfoil but higher than the S406 airfoil for the lower Reynolds number. For the higher Reynolds number, the S414 airfoil still exhibits lower profile-drag coefficients than the S411 airfoil but similar profile-drag coefficients to the S406 airfoil. For both cases, the S414 airfoil shows substantially more-negative pitching-moment coefficients and more-abrupt stall characteristics than both single-element airfoils. The maximum lift coefficient is over 40% higher than the other two airfoils for $R = 0.7 \times 10^6$ and over 50% higher for $R = 1.5 \times 10^6$; however, the S414 exhibits a much more abrupt stall. These trends, including the significantly higher maximum lift coefficient, hold for the other Reynolds numbers tested [4–6].

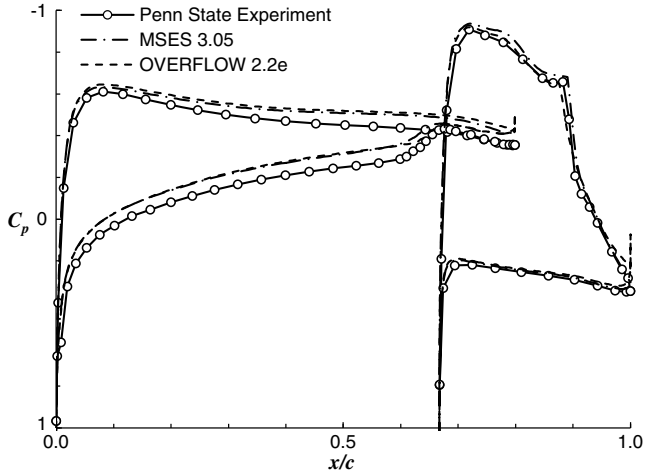

Fig. 11 Comparison of theoretical and experimental pressure distributions at $c_l = 0.493$ for $R = 0.7 \times 10^6$.

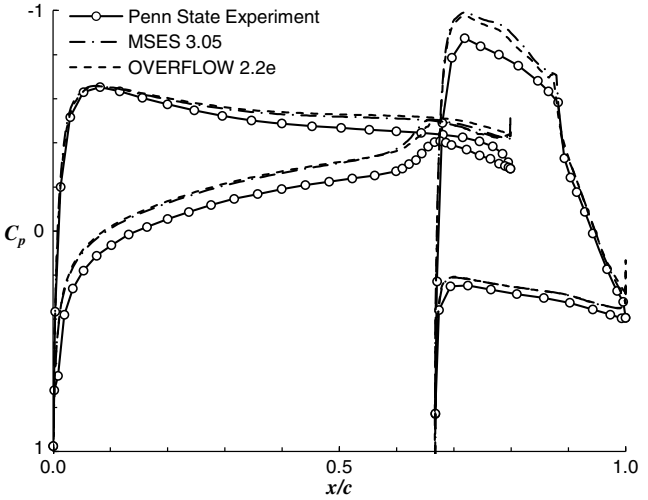

Fig. 12 Comparison of theoretical and experimental pressure distributions at $c_l = 0.518$ for $R = 1.5 \times 10^6$.

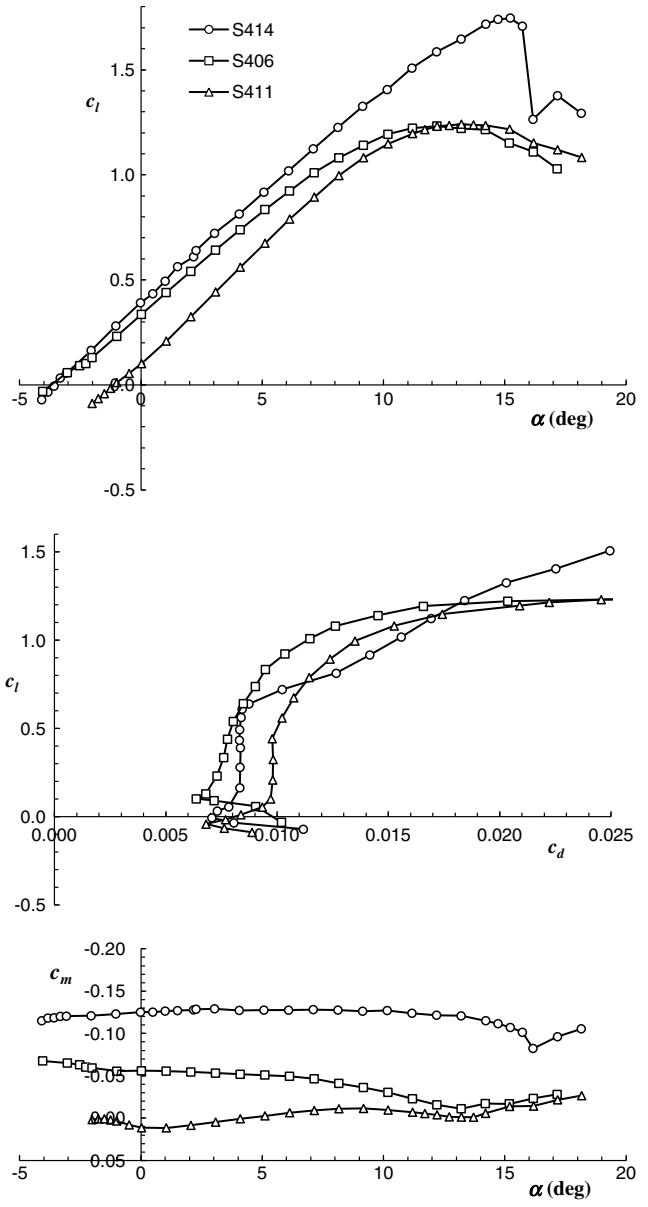

Fig. 13 Comparison of measured section characteristics for the S414, S406, and S411 airfoils for $R = 0.7 \times 10^6$.

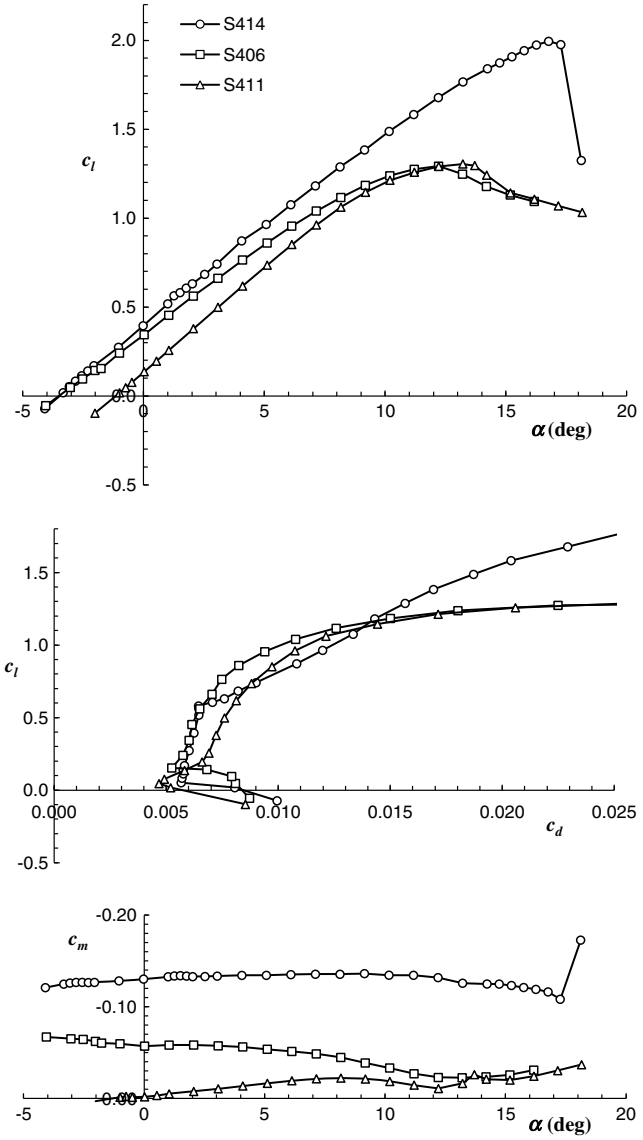

Fig. 14 Comparison of measured section characteristics for the S414, S406, and S411 airfoils for $R = 1.5 \times 10^6$.

VII. Conclusions

The S414, a 14.22%-thick, slotted, natural-laminar-flow (SNLF) airfoil intended for rotorcraft applications, has been theoretically analyzed using the MSES and OVERFLOW codes and experimentally investigated in the Penn State University Low-Speed, Low-Turbulence Wind Tunnel. The experimental results show that the primary design objectives of a high maximum lift coefficient and low profile-drag coefficients were achieved, although the airfoil exhibits abrupt stall characteristics. The comparisons of the theoretical predictions and experimental measurements show good agreement overall. Comparisons of the S414 airfoil with the S406 and S411 airfoils, which are single-element airfoils designed to similar specifications, illustrate the potential benefits of the SNLF concept.

Acknowledgments

The airfoils used in this study were designed and tested as part of an effort sponsored by the U.S. Army with Preston B. Martin serving as the technical monitor. All computational fluid dynamics analyses were performed on systems maintained by the Pennsylvania State University Research Computing and Cyberinfrastructure Group.

References

[1] Somers, D. M., "Laminar-Flow Airfoil," U.S. Patent 6,905,092 B2, June 2005.

[2] Somers, D. M., "An Exploratory Investigation of a Slotted, Natural-Laminar-Flow Airfoil," NASA CR-2012-217560, 2012.

[3] Whitcomb, R. T., and Clark, L. R., "An Airfoil Shape for Efficient Flight at Supercritical Mach Numbers," NASA TM-X-1109, 1965.

[4] Somers, D. M., and Maughmer, M. D., "Design and Experimental Results for the S414 Airfoil," U.S. Army Research, Development and Engineering Command TR-10-D-112, Aberdeen Proving Ground, MD, 2010.

[5] Somers, D. M., and Maughmer, M. D., "Design and Experimental Results for the S406 Airfoil," U.S. Army Research, Development and Engineering Command TR-10-D-107, Aberdeen Proving Ground, MD, 2010.

[6] Somers, D. M., and Maughmer, M. D., "Design and Experimental Results for the S411 Airfoil," U.S. Army Research, Development and Engineering Command TR-10-D-111, Aberdeen Proving Ground, MD, 2010.

[7] Eppler, R., *Airfoil Design and Data*, Springer–Verlag, Berlin, 1990, pp. 82–87.

[8] Eppler, R., "Airfoil Program System 'PROFIL07' User's Guide," Stuttgart, Germany, 2007.

[9] Drela, M., "A User's Guide to MSES 3.05," Massachusetts Inst. of Technology, Cambridge, MA, 2007.

[10] Drela, M., "Implicit Implementation of the Full e^n Transition Criterion," *21st AIAA Applied Aerodynamics Conference*, AIAA Paper 2003-4066, June 2003.
doi:10.2514/6.2003-4066

[11] Drela, M., and Giles, M. B., "Viscous-Inviscid Analysis of Transonic and Low Reynolds Number Airfoils," *AIAA Journal*, Vol. 25, No. 10, 1987, pp. 1347–1355.
doi:10.2514/3.9789

[12] Nichols, R., and Buning, P. G., "User's Manual for OVERFLOW 2.1, Version 2.1t," NASA Langley Research Center, Hampton, VA, August 2008.

[13] Roe, P. L., "Approximate Riemann Solvers, Parameter Vectors, and Difference Schemes," *Journal of Computational Physics*, Vol. 43, No. 2, 1981, pp. 357–372.
doi:10.1016/0021-9991(81)90128-5

[14] Pulliam, T. H., and Chaussee, D. S., "A Diagonalized Form of an Implicit Approximate Factorization Algorithm," *Journal of Computational Physics*, Vol. 39, No. 2, Feb. 1981, pp. 347–363.
doi:10.1016/0021-9991(81)90156-X

[15] Pandya, S., Venkateswaran, S., and Pulliam, T. H., "Implementation of Preconditioned Dual-Time Procedures in OVERFLOW," *41st Aerospace Sciences Meeting and Exhibit*, AIAA Paper 2003-0072, Jan. 2003.
doi:10.2514/6.2003-72

[16] Spalart, P. R., and Allmaras, S. R., "A One-Equation Turbulence Model for Aerodynamic Flows," *30th AIAA Aerospace Sciences Meeting and Exhibit*, AIAA Paper 1992-0439, Jan. 1992.
doi:10.2514/6.1992-439

[17] Coder, J. G., and Maughmer, M. D., "A CFD-Compatible Transition Model Using an Amplification Factor Transport Equation," *51st Aerospace Sciences Meeting and Exhibit*, AIAA Paper 2013-0253, Jan. 2013.
doi:10.2514/6.2013-253

[18] Chan, W. M., Rogers, S. E., Nash, S. M., Buning, P. G., Meakin, R. L., Boger, D. A., and Pandya, S., "Chimera Grid Tools User's Manual, Version 2.0," NASA Ames Research Center, Mountain View, CA, July 2007.

[19] Chan, W. M., Gomez, R. J., Rogers, S. E., and Buning, P. G., "Best Practices in Overset Grid Generation," *32nd AIAA Fluid Dynamics Conference*, AIAA Paper 2002-3191, June 2002.
doi:10.2514/6.2002-3191

[20] Premi, A., Maughmer, M. D., and Brophy, C. M., "Flow-Quality Measurements and Qualification of the Pennsylvania State University Low-Speed, Low-Turbulence Wind Tunnel," *50th AIAA Aerospace Sciences Meeting and Exhibit*, AIAA Paper 2012-1214, Jan. 2012.
doi:10.2514/6.2012-1214

[21] Prankhurst, R. C., and Holder, D. W., *Wind-Tunnel Technique*, Sir Isaac Pitman & Sons, London, 1965, pp. 274–283.

[22] Allen, H. J., and Vincenti, W. G., "Wall Interference in a Two-Dimensional-Flow Wind Tunnel, with Consideration of the Effect of Compressibility," NACA, Rept. 782, 1944.

[23] "Assessment of Experimental Uncertainty with Application to Wind Tunnel Testing," AIAA Standard S-071A-1999, Rev. A, AIAA, Reston, VA, 1999.

[24] Loving, D. L., and Katzoff, S., "The Fluorescent-Oil Film Method and Other Techniques for Boundary-Layer Flow Visualization," NASA Memorandum 3-17-59L, 1959.

[25] McGhee, R. J., Beasley, W. D., and Foster, J. M., "Recent Modifications and Calibration of the Langley Low-Turbulence Pressure Tunnel," NASA TP-2328, 1984.

[26] van Ingen, J. L., Boermans, L. M. M., and Blom, J. J. H., "Low-Speed Airfoil Section Research at Delft University of Technology," *12th Congress of the International Council of the Aeronautical Sciences*, Paper ICAS-80-10.1, Munich, Oct. 1980.

[27] Somers, D. M., and Maughmer, M. D., "Experimental Results for the E 387 Airfoil at Low Reynolds Numbers in The Pennsylvania State University Low-Speed, Low-Turbulence Wind Tunnel," U.S. Army Research, Development and Engineering Command TR-07-D-32, Aberdeen Proving Ground, MD, May 2007.

[28] Medina, R., "Validation of The Pennsylvania State University Low-Speed, Low-Turbulence Wind Tunnel Using Measurements of the S805 Airfoil," M.S. Thesis, Dept. of Aerospace Engineering, Pennsylvania State Univ., University Park, PA, 1994.

[29] McGhee, R. J., Walker, B. S., and Millard, B. F., "Experimental Results for the Eppler 387 Airfoil at Low Reynolds Numbers in the Langley Low-Turbulence Pressure Tunnel," NASA TM-4062, Oct. 1988.

[30] Somers, D. M., "Design and Experimental Results for the S805 Airfoil," National Renewable Energy Lab., Rept. SR-440-6917, Golden, CO, Oct. 1988.